Journal of Medicinal Chemistry

Article

pubs.acs.org/jmc

Pyrrolopyrazines as Selective Spleen Tyrosine Kinase Inhibitors

Fernando Padilla,*[,†] Niala Bhagirath,[†] Shaoqing Chen,[†] Eric Chiao,[†] David M. Goldstein,[†,∥] Johannes C. Hermann,[†] Jonathan Hsu,[†] Joshua J. Kennedy-Smith,[†] Andreas Kuglstatter,[†] Cheng Liao,[†] Wenjian Liu,[‡] Lee E. Lowrie, Jr.,[†] Kin Chun Luk,[†] Stephen M. Lynch,[†] John Menke,[†] Linghao Niu,[†] Timothy D. Owens,[†] Counde O-Yang,[‡] Aruna Railkar,[†] Ryan C. Schoenfeld,[†] Michelle Slade,[†] Sandra Steiner,[†] Yun-Chou Tan,[†] Armando G. Villaseñor,[†] Ce Wang,[‡] Jutta Wanner,[†] Wenwei Xie,[‡] Daigen Xu,[†] Xiaohu Zhang,[‡,⊥] Mingyan Zhou,[†] and Matthew C. Lucas*[,†,§]

[†]Hoffmann-La Roche Inc., pRED, Pharma Research & Early Development, 340 Kingsland Street, Nutley, New Jersey 07110, United States

[‡]BioDuro Beijing Co. Ltd., Building E, No. 29, Life Science Park Road, Changping District, Beijing 102206, P.R. China

Supporting Information

ABSTRACT: We describe the discovery of several pyrrolopyrazines as potent and selective Syk inhibitors and the efforts that eventually led to the desired improvements in physicochemical properties and human whole blood potencies. Ultimately, our mouse model revealed unexpected toxicity that precluded us from further advancing this series.

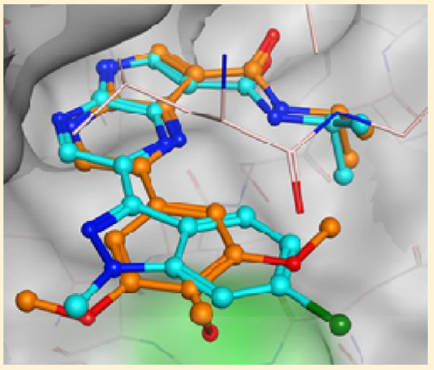

INTRODUCTION

Protein kinases constitute one of the largest families of human enzymes and regulate many different signaling processes by appending phosphate groups to proteins. Tyrosine kinases, in particular, phosphorylate proteins on the alcohol moiety of tyrosine residues. The tyrosine kinase family includes members that control cell growth, migration, and differentiation.[1] Abnormal kinase activity has been implicated in a variety of human diseases including cancers and autoimmune and inflammatory diseases.[2] Because protein kinases are among the key regulators of cell signaling, they are attractive drug targets, and selective and efficacious kinase inhibitors provide a means to modulate cellular function. These inhibitors are not only relevant for the treatment of kinase-mediated disease processes but are also highly useful for investigation of cell signaling processes and the identification of other cellular targets of therapeutic interest.

Spleen tyrosine kinase (Syk) inhibitors possess a high potential for the treatment of inflammatory and autoimmune disorders.[3] This cytoplasmic protein kinase, discovered in 1991,[4] associates with receptors on the surface of immune cells including B cells, mast cells, macrophages, and neutrophils, and nonimmune cells such as osteoclasts.[5] The engagement of these receptors with their ligands activates Syk, which in turn orchestrates different cellular processes, including cytokine production (in T cells and monocytes), bone resorption (in osteoclasts), and phagocytosis (in macrophages).[6] In addition, because Syk is positioned upstream in the cell signaling pathway, therapies targeting Syk might be more advantageous than drugs that inhibit a single downstream event.[7]

Syk's potential as a therapeutic target for an array of inflammatory diseases has led to many pharmaceutical companies, as well as academic institutions, becoming involved in the development of inhibitors of Syk. Fostamatinib (**1**, Figure 1), a Syk inhibitor, has demonstrated in phase 2 studies that it can reduce disease activity in patients with rheumatoid arthritis (RA). However, it showed adverse events including diarrhea, hypertension, and neutropenia.[8] A more selective inhibitor **2** is currently in phase 2, but safety data has not yet been reported.[9] We, and others, have commented that some of the observed side effects of **1** are likely due to off-target activities and that inhibitors with an enhanced selectivity profile compared to that shown by **1** might improve the safety profile.[9,10] The availability of a compound with such selectivity will facilitate further evaluation of Syk as a target for the treatment of diseases such as rheumatoid arthritis, asthma, systemic lupus erythematosus (SLE), idiopathic thrombocytopenic purpura (ITP),

Received: November 21, 2012
Published: January 28, 2013

dx.doi.org/10.1021/jm301720p | J. Med. Chem. 2013, 56, 1677−1692

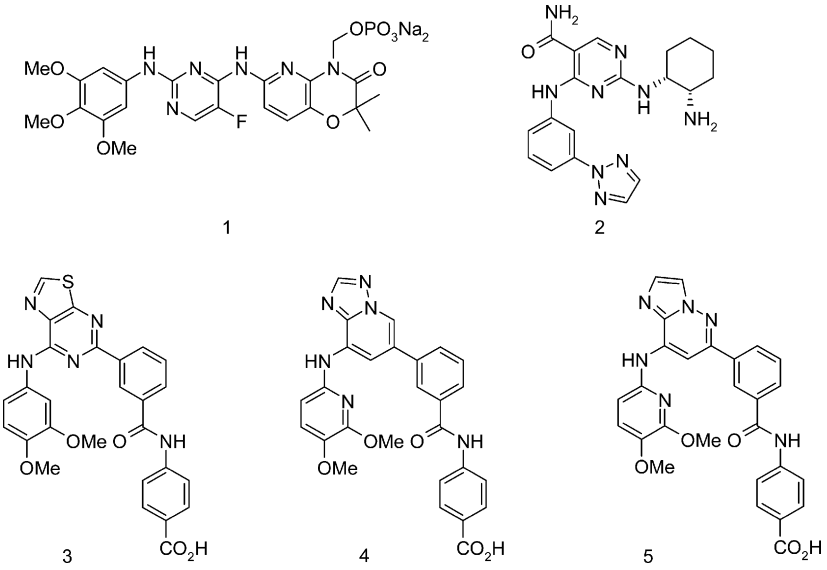

Figure 1. Fostamatinib **1**, PRT-062607 **2**, and selective Syk inhibitors **3**−**5**.

Crohn's disease, allergic rhinitis, multiple sclerosis, leukemia, and carcinomas.[3]

DISCUSSION

Our earliest efforts to develop small molecule Syk inhibitors (**3**−**5**, Figure 1) were successful with respect to finding potent scaffolds with excellent selectivity profiles, yet their poor physicochemical properties prevented us from assessing them in in vivo models of RA.[9] As a consequence, we sought new chemical scaffolds as starting points with similar potency and selectivity but with improved potential to achieve the biopharmaceutical properties required to deliver orally available drug molecules. The pyrrolopyrazine scaffold (e.g., **6**, Figure 2) had been previously identified by us as a Syk/Jak kinase inhibitor platform.[11] The pyrrolopyrazines were revisited as a starting point in our effort to find Syk-specific inhibitors because of their good ligand efficiency (ligand efficiency data not shown) and high permeability, two qualities that had proved elusive in some of our early scaffolds (**3**−**5**). On the basis of our newly developed insight into how to obtain good Syk selectivity profiles,[9] we felt that there were new opportunities to rationally introduce selectivity into the scaffold. In short, we had identified four amino acid residues that rarely appeared in other kinase active sites: Met450, Leu453, Pro455, and Asn457 (each having an incidence in less than 5% of all kinases). Of these, we had demonstrated that optimizing interactions of ATP-competitive Syk inhibitors with Pro455, present in only nine aligned kinases of a total of 433, was an attractive way of introducing high levels of Syk specificity.

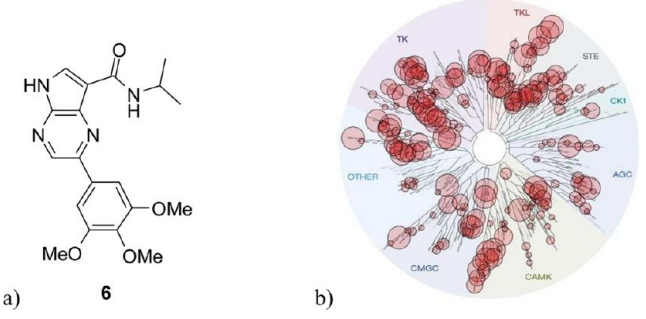

Figure 2. (a) Pyrrolopyrazine kinase inhibitor **6**; (b) DiscoverX kinase screening dendrogram for **6** at 10 μM concentration. The KINOMEscan screening platform employs an active site-directed competition binding assay to quantitatively measure interactions between test compounds and 386 kinase assays. Images generated using TREE*spot* Software Tool. Reprinted with permission from KINOME*scan*, a division of DiscoveRx Corporation, 2010.

RESULTS

The pyrrolopyrazine lead molecule **6** showed good permeability, very attractive ligand efficiency, and excellent cell-based potency (Tables 2, 3). It also had a potency in our human whole blood (HWB) assay that was superior to that of **1** (Tables 1, 2). The high human whole blood potency was very appealing to us because we consider HWB potency as an excellent predictor for efficacy in the clinic, and obtaining good HWB activity had been a significant challenge during our optimization of compounds such as **3**−**5**. Early on, we identified some challenges with the pyrrolopyrazine scaffold that needed to be addressed, including a poor selectivity profile (Figure 2b and Table 2) and the formation of GSH adducts during in vitro incubation with human liver microsomes (e.g., **7**, Table 3). At the outset, though, we were optimistic

Table 1. Inhibition of Syk Activity, Selectivity, and Human Whole Blood Potency of Compounds 1−3

compd	Syk IC_{50}[a] (nM)	JAK3 selectivity	JAK2 selectivity	JAK1 selectivity	kinase selectivity[b]	B cell IC_{50}[c] (μM)	HWB IC_{50}[d] (μM)
1	17	2	0.1	0.4	145/290	0.267	12.0
2	1	>1000	>700	>300	116/385	0.223	0.540
3	7	>139	63	561	14/386	0.156	11.9

[a]See Experimental Section for details. [b]DiscoverX kinase screening dendrogram (number of kinases inhibited >90% at 10 μM). The KINOMEscan screening platform employs an active site-directed competition binding assay to quantitatively measure interactions between test compounds and multiple kinase assays. [c]Ramos B cell IC_{50}. [d]Human whole blood IC_{50}.

dx.doi.org/10.1021/jm301720p | J. Med. Chem. 2013, 56, 1677−1692

that these challenges could be overcome. First, on the basis of our analysis of an X-ray structure on the initial lead **6** and our experience with previous scaffolds,[11] we expected that replacement or modification of the phenyl ring to optimize interaction with Pro455 would improve the selectivity of the compounds (Figure 3). Second, the GSH adduct formation observed for **7** was not

Table 2. Inhibition of Syk Activity, Selectivity, B cell Potency, Human Whole Blood Potency, and clogP Values for Pyrrolopyrazines 6−18

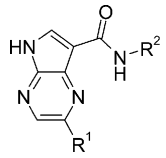

Compound	R^1	R^2	Syk IC_{50}[a] (nM)	Kinase Selectivity[b]	B cell IC_{50}[c] (μM)	HWB IC_{50}[d] (μM)	clogP[e]
6	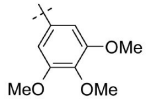	^{i}Pr	14	156/293	0.190	7.09	2.42
7	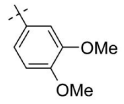		35	-	0.256	0.911	1.63
8	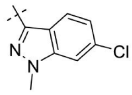	^{i}Pr	36	9/386	0.512	16.6	3.48
9	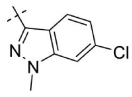	^{t}Bu	7	2/386	>31	>50	3.87
10	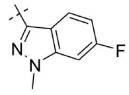	^{t}Bu	4	-	0.252	-	3.30
11	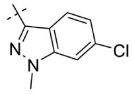		13	32/386	0.291	4.85	2.39
12	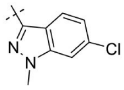		6	10/385	0.240	6.48	2.78
13	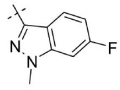	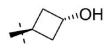	47	-	0.151	1.43	2.45
14	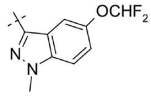	^{t}Bu	1	7/385	0.179	2.58	3.69
15	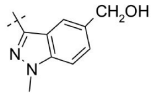	^{t}Bu	5	-	0.119	0.839	2.12
16	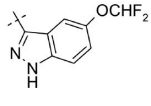	^{t}Bu	2	-	0.088	2.45	3.95

dx.doi.org/10.1021/jm301720p | J. Med. Chem. 2013, 56, 1677−1692

Table 2. continued

Compound	R^1	R^2	Syk IC_{50}[a] (nM)	Kinase Selectivity[b]	B cell IC_{50}[c] (μM)	HWB IC_{50}[d] (μM)	clogP[e]
17	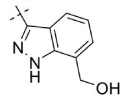	^{t}Bu	3	-	0.086	0.412	2.23
18	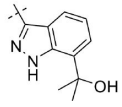	^{t}Bu	10	-	0.076	0.534	2.93

[a]See Experimental Section for details. [b]DiscoverX kinase screening dendrogram (number of kinases inhibited >90% at 10 μM). The KINOMEscan screening platform employs an active site-directed competition binding assay to quantitatively measure interactions between test compounds and multiple kinase assays. [c]Ramos B cell IC_{50}. [d]Human whole blood IC_{50}. [e]Calculated log *P*.

Table 3. Solubility[a], Permeability[b], Human Plasma Protein Binding[c], CYP450 Inhibition[d], and Liver Microsomal Stability[e,f], hERG Channel Inhibition[g], and GSH-Adduct Formation[h]

compd	LYSA[a] (μg/mL)	CACO2 AB (ER)[b]	PPB (% free)[c]	CYP450 IC_{50} (μM)[d]	HLM[e]	RLM[f]	hERG IC_{50} (μM)[g]	GSH[h]
1	<1	16	1.5	>50	18	47	>1	yes
2	<1	0.4	1.4	>25	3	10	9.1	no
3	<1	0	0.94	>50				
6		15	<1	16 (2C9)	14	42		
7	2	2	4	>50				yes
8		0.2			1	32		no
9	<1	0.2	0.3	>50				no
10	<1	0.2	0.14		14	48		
11	<1	1.8	0.8		16	47		no
12	<1	9	0.3	>7	14	44		no
13	<1			>50	17	43		
14	<1		0.1	>19	18	51		
15	<1	8		>8 (2D6)	17	41		yes
16	<1			>19	10	30		no
17	<1			12 (2D6)	7	51		
18	5	2		5 (2D6)	2	47	>2	

[a]Lyophilized solubility assay. [b]Apical to basolateral CACO2 permeability, followed by measured efflux ratio. [c]Human plasma protein binding % free fraction. [d]CYP450 inhibition at isoforms 3A4, 2C9, and 2D6. Isoform with the highest percent inhibition listed. [e]Stability in human liver microsomes (mL/min/kg). [f]Stability in rat liver microsomes (mL/min/kg). [g]hERG channel binding. [h]GSH adduct formation flag.

unexpected due to the presence of the dimethoxyphenyl front group. Compound **7** also showed low plasma protein binding, an attribute that we felt might be critical in our quest to obtain good potency in the human whole blood assay. Indeed, compound **7** had HWB potency values within 2-fold of competitor molecule **2**.

Molecular modeling was used to seek ways of optimizing interactions with Pro455. Among the replacements for the phenyl front group that were modeled and docked, we felt that bicyclic heteroaromatic systems showed particularly strong potential to improve the van der Waals interactions with Pro455, and therefore exhibit enhanced selectivity profiles. From rigorous mining of our internal database of JAK inhibitor compounds, we knew that the pyrrolopyrazine scaffold also had the propensity to inhibit Syk. Further analysis helped us to identify a handful of compounds that possessed some of the heterocyclic replacements with the best fit based on modeling. Indazoles, such as compound **8** in Figure 3, were particularly appealing. As previously reported by our group,[12] the lowest energy conformation of the indazole core (Figure 4) is predicted to favor the desirable van der Waals interaction with Pro455.

5-Chloroindazole, analogue **8**, showed in on our modeling studies a good steric fit for optimal van der Waals interactions with Pro455. The good fit prediction was confirmed by the observed high potency as a Syk inhibitor in vitro (Table 2). On further profiling, we were excited to find that **8** had a superior in vitro profile overall when compared to compound **6**. It not only showed vastly improved kinase selectivity (Table 2), but in addition it showed no glutathione adduct formation in vitro (Table 3). We obtained an X-ray crystal structure of **8** that confirmed the predicted binding mode and suggested that optimal interactions with the Pro455 were driving the observed selectivity because all other interactions appeared unchanged compared to **6** (Figure 3). That the crystal structure supported our selectivity hypothesis encouraged further optimization of this scaffold. Our renewed enthusiasm for the scaffold was sustained when we found that **8** had a potency of ∼16 μM in the HWB assay. This value was close to that measured for **1** and certainly appeared within reach of **2**.

Our profiling also clearly highlighted areas in which further optimization efforts were needed. Solubility was a major concern, and despite having significantly improved selectivity over the kinome, reducing the potent JAK family activity was important (e.g., compound **8** was 0.2-, 1-, and 2-fold selective over JAK3, JAK2, and JAK1, respectively). Although there is evidence to

dx.doi.org/10.1021/jm301720p | J. Med. Chem. 2013, 56, 1677−1692

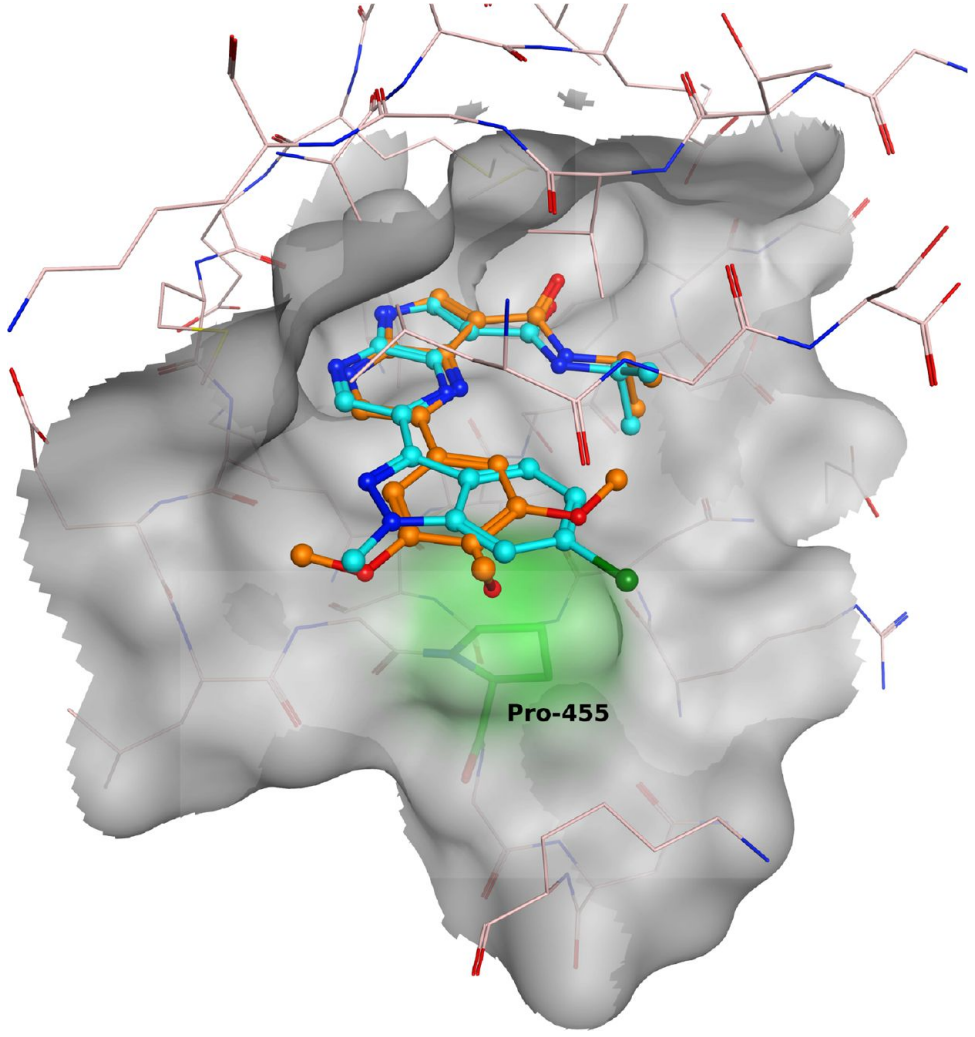

Figure 3. Crystal structure of compound **6** in complex with Syk (PDB accession number 4I0R, 2.1 Å resolution). Carbon atoms of the protein are colored in pink and compound carbon atoms colored in orange (**6**). Overlayed is compound **8** in cyan (PDB 4I0S, 1.98 Å resolution). Nitrogen atoms are colored in blue and oxygen atoms in red. Proline 455 is highlighted with carbon colored in green. All molecular visualizations are generated with MOE.[13].

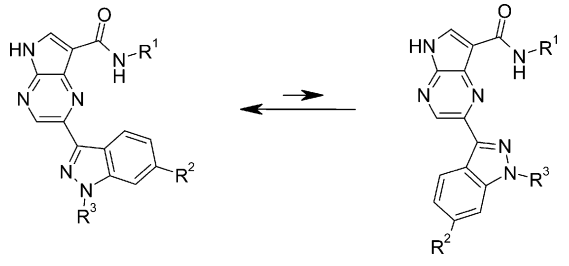

Figure 4. Preferred conformation of the indazole pyrazine core.

suggest that a combination of Syk and JAK inhibition might lead to greater efficacy in vivo (for example, Rigel's Fostamatinib inhibits JAK as well as Syk, and Pfizer's Tofacitinib is a pan-JAK kinase inhibitor that shows strong efficacy in phase III clinical trials for RA),[14] our goal was to increase the selectivity for Syk over the JAK family, as well as other kinases, to improve our chances of delivering a clinically differentiated medicine.

Because the indazole moiety had provided such an excellent boost to selectivity over the kinome, we first maintained this group relatively constant and directed our initial optimization efforts toward the amide moiety. Many of the earliest examples in this pyrrolopyrazine scaffold, which contained phenyl substituents rather than the indazole moieties, had previously been assessed for kinase selectivity in a small panel of 40 kinases which included both Syk and JAK3. Data mining and analysis of this selectivity data for a number of matched pairs suggested that an increase in the steric bulk at the amide portion should manifest itself through a favorable increase in selectivity over JAK3 and, presumably, the other JAK family members. Thus, starting with the isopropyl amide as our benchmark, we made the next logical step and synthesized the *t*-butyl amide compound **9** and then related analogue **10**. Gratifyingly, potency for Syk was improved, outstanding selectivity over the kinome was obtained (Figure 5), and most importantly, reduced inhibition of the JAK family of kinases was observed (e.g., **9** showed 61-, 250-, and >1373-fold selectivity for Syk over JAK3, JAK2, and JAK1, respectively). However, further profiling of **9** showed that it had no potency in either the cell-based assay or the HWB assay (Table 2). We attributed the lack of activity in these assays to poor properties due to its elevated lipophilicity (clogP = 3.9). Thus we pursued amide substituents that would lower the clogP into a more desirable range. We investigated the introduction of a hydroxyl group first because the early SAR suggested this could positively impact properties and improve human whole blood potency (for example, compare **6** and **7**, Table 2). Compound **11** was

dx.doi.org/10.1021/jm301720p | *J. Med. Chem.* 2013, 56, 1677−1692

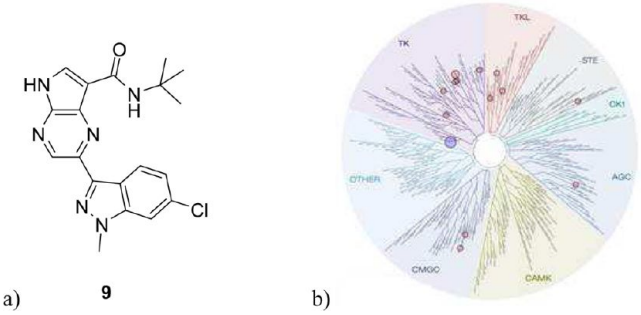

Figure 5. (a) Pyrrolopyrazine kinase inhibitor **9**; (b) DiscoverX kinase screening dendrogram for **9** at 10 μM concentration. The KINOMEscan screening platform employs an active site-directed competition binding assay to quantitatively measure interactions between test compounds and 386 kinase assays. Images generated using TREE*spot* Software Tool. Reprinted with permission from KINOME*scan*, a division of DiscoveRx Corporation, 2010.

prepared and did show significantly improved HWB potency. Permeability improved slightly, and plasma protein binding was acceptable, suggesting that the improved physicochemical properties were important contributors to achieving better human whole blood potency. Next, we evaluated the 2-hydroxy-1,1-dimethyl-ethyl amide analogue **12**. This modification also resulted in a large improvement in HWB potency, and we were pleased that the selectivity over the JAK family remained respectable (12-, 35-, and 34-fold over JAK3, JAK2, and JAK1, respectively). We were further encouraged by analogue **13**, which showed very good cell and HWB potency. Thus, we determined that bulky amide substituents were required to ensure that we obtained Syk selectivity over the JAK family, and that the addition of polar functionality could improve the HWB potency, presumably through lowering clogP and improving overall physicochemical properties.

SAR with respect to indazole substituents was also assessed, and selected results are highlighted in Tables 2 and 3. In summary, substituents of various sizes and electronics in the 5-, 6-, and 7-position were well tolerated. Similar to what we had observed with the amide modifications, reduction of the clogP generally improved whole blood potencies. For example, compound **15** showed submicromolar activities in the HWB assay. Demethylation of the indazoles to expose the polar indazole hydrogen offered an alternative way of reducing the clogP (**16**–**18**, Table 2) and led to the identification of **17**, a very potent compound in the HWB assay (IC_{50} = 412 nM).

Unfortunately, despite the improved clogP for these compounds (Table 2), all representatives that were tested showed poor oral bioavailability as assessed in rodent single-dose PK studies (e.g., **15**, Table 8). Because most of these examples had moderate or good permeability but very low solubility, we also sought to improve the solubility by disrupting the aromatic π-stacking ability of these planar molecules by substituting at the benzylic position. Doing so generated **18**, which had excellent cell potency and HWB potency. However, essentially no improvement in solubility was achieved, and the PK data showed, not surprisingly, only very minor improvements (Table 8).

Seeking a greater impact on solubility in order to obtain compounds with balanced PK/potency profiles, we implemented the following strategies:

(1) The introduction of basic functionalities at the amide substituent (**19**–**25**, Table 4).

(2) The introduction of polar or basic groups that might project out of the binding pocket into bulk solvent at the indazole nitrogen (**26**–**38**, Table 4).

(3) The reduction in sp2 carbon count (**39**–**40**, Table 4).

Introduction of basicity at the amide substituent proved to be a somewhat successful strategy for improving solubility. For many compounds, improved solubility was achieved while maintaining reasonable HWB potency (for example, compounds **20**, **21**, and **24**, Tables 4 and 5). The amines were selected based on modeling studies that suggested that the amine functionality should be tolerated at the specific position. We were pleased that these changes were usually also accompanied by improved stability in HLM and RLM (Table 5).

Compound **24** showed excellent selectivity on further profiling, and no human ether-a-go-go-related gene (hERG) channel inhibition was detected. Several of these analogues were assessed in SDPK experiments, and, unfortunately, all showed very low oral bioavailability (e.g., **24**, Table 8). This might be due to the fact that the permeability of these compounds, with the additional hydrogen bond donors and the positive charge at physiological pH, was generally very poor.

The results of our alternative efforts of introducing a solvent-exposed amine via a flexible linker or as a cyclic amine, and of introducing polar groups via flexible linkers to the indazole N-1 position, are also shown in Tables 4 and 5. Although we did not see the solubility improvement that we had anticipated, in some cases we observed significantly enhanced HWB potencies while maintaining excellent to good selectivity profiles (e.g., **26** and **31**, Table 4). In contrast to the basic amines at the amide position, which had been free from a cardiovascular toxicity flag in the hERG assay, these compounds showed remarkably high, and consequently unacceptable, inhibition of the hERG channel. Inhibition of the hERG channel has been associated with QT prolongation and fatal arrhythmias.[15]

Because the overall profile of these compounds looked promising, we embarked on an exploration of ways to reduce the hERG binding affinity. In the case of the amine-containing compounds, we investigated reducing the basicity of the amine. This is a strategy that has improved countless series for many discovery groups including our own,[16] and examples of some of the compounds with attenuated basicity are shown (**28**–**29**, Table 4). We were disappointed to find that lowering the pK_a did not translate into improved hERG safety. For example, 3-cyanoazetidine compound **28** and morpholino analogue **29** showed only minimal reduction of the hERG signal while maintaining good HWB potencies.

We next investigated whether the amphiphilicity of these compounds was contributing to the high hERG channel blocking effect. When we replaced the hydrophobic *tert*-butyl amide with the more hydrophilic *N*-(3-hydroxy-2,2-dimethyl-propyl) amide to obtain **30**, we were pleased to find that a substantial reduction of the hERG signal was achieved. However, although the cardiovascular toxicity risk had been reduced, it remained higher than we were comfortable with, and we continued our search for compounds with an improved therapeutic window.

Results from mutagenesis and molecular modeling studies have shown that aromatic substitutions can strongly influence interactions with the hERG receptor.[17] Thus, while we had been very encouraged by the higher potency in HWB of the $OCHF_2$ group, we investigated some of the alternative substituents on the indazole that we had previously identified in order to evaluate whether the indazole-$OCHF_2$ moiety could be acting as some

kind of recognition motif for the hERG channel. A comparison of compounds **30** with **37** and **31** with **33** (Table 5), for example, suggested that the 5-difluoromethoxy group was indeed responsible for much of the hERG activity. Thus, we moved away from this substituent. We also prepared molecules where the amine was part of a five- or six-membered ring directly attached to the N-1 position of the indazole (e.g., **38**, Table 4). We anticipated that in addition to potentially impacting

Table 4. Inhibition of Syk Activity, Selectivity, Human Whole Blood Potencies, and clogP Values for Pyrrolopyrazines 19−40

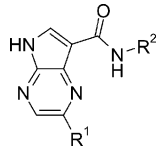

Compound	R^1	R^2	Syk IC_{50}[a] (nM)	Kinase Selectivity[b]	B cell IC_{50}[c] (μM)	HWB IC_{50}[d] (μM)	clogP[e]
19	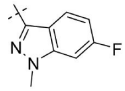		64	-	3.70	-	2.20
20	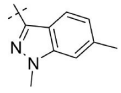		34	-	1.31	1.77	2.82
21	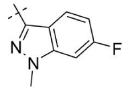	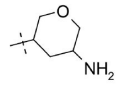	61	-	1.477	0.643	1.96
22	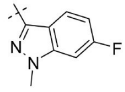	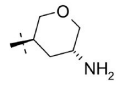	13 5	-	1.841	0.376	1.96
23	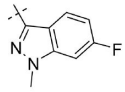	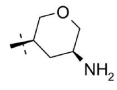	68	-	1.371	1.16	1.96
24	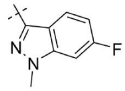	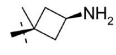	4	3/386[f]	0.848	0.581	2.85
25	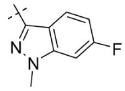	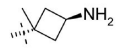	10	-	3.69	0.427	2.85
26	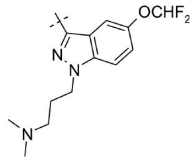	^{t}Bu	5	70/386	0.140	0.184	4.15
27	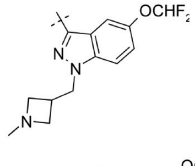	^{t}Bu	19	-	2.79	0.546	4.03
28	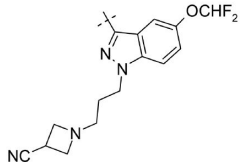	^{t}Bu	4	-	0.211	0.534	4.06

dx.doi.org/10.1021/jm301720p | J. Med. Chem. 2013, 56, 1677−1692

Table 4. continued

Compound	R^1	R^2	Syk IC_{50}[a] (nM)	Kinase Selectivity[b]	B cell IC_{50}[c] (μM)	HWB IC_{50}[d] (μM)	clogP[e]
29	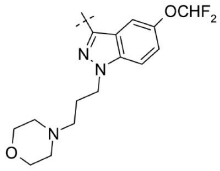	^{t}Bu	3	-	0.195	0.277	4.08
30	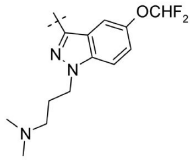		30	-	0.127	0.101	3.06
31	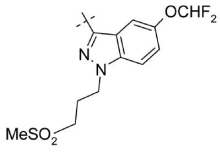	^{t}Bu	3	10/386[f]	0.170	0.335	2.75
32	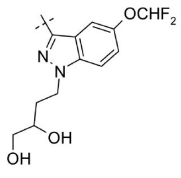	^{t}Bu	2	-	0.080	0.534	2.44
33	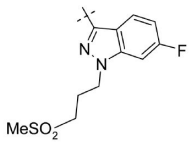	^{t}Bu	5	-	0.057	0.285	2.36
34	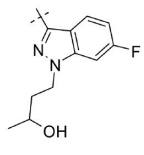		16	-	-	0.563	2.09
35	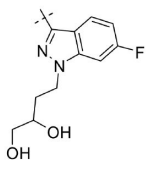	^{t}Bu	5	-	0.366	0.360	2.05
36	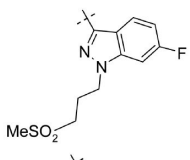		16		0.078	0.094	1.27
37	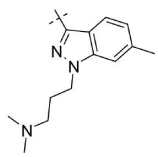		68	-	6.92	0.191	3.03

dx.doi.org/10.1021/jm301720p | J. Med. Chem. 2013, 56, 1677−1692

Table 4. continued

Compound	R^1	R^2	Syk IC_{50}[a] (nM)	Kinase Selectivity[b]	B cell IC_{50}[c] (μM)	HWB IC_{50}[d] (μM)	clogP[e]
38	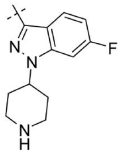	^{t}Bu	4	-	0.142	0.852	2.92
39	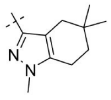	^{i}Pr	13 2	-	0.738	-	3.53
40		^{t}Bu	26	35/386[f]	0.450	0.634	2.32

[a]See Experimental Section for details. [b]DiscoverX kinase screening dendrogram (number of kinases inhibited >90% at 10 μM). The KINOMEscan screening platform employs an active site-directed competition binding assay to quantitatively measure interactions between test compounds and multiple kinase assays. [c]Ramos B cell IC_{50}. [d]Human whole blood IC_{50}. [e]Calculated log *P*. [f]Tested at 1 μM concentration.

Table 5. Solubility[a], Permeability[b], Human Plasma Protein Binding[c], CYP450 Inhibition[d], Liver Microsomal Stability[e,f], hERG Channel Inhibition[g], GSH-Adduct Formation[h], and cpKa[i]

compd	LYSA[a] (μg/mL)	CACO2 AB (ER)[b]	PPB (% free)[c]	CYP450 IC_{50} (μM)[d]	HLM[e]	RLM[f]	hERG IC_{50}[g] (μM)	GSH[h]	cpKa[i]
19	<1	3		>50	12	25			
20	429	0.1	4	3 (2D6)	5	15			
21	101			>50	5	19			
22		0.2			2	23			
23					4	26			
24	10	0.1	8	4 (2C9)	2	13	>30	no	
25	3	0.1		>50	2	0	>1		
26	<1			>50	9	46	<0.3	no	9.36
27	<1	0.2	1.1	19 (2D6)	5	17	0.293	no	
28	<1	28		5 (2C9)	20	58	0.414		6.41
29	<1	1.3		4 (2C9)	20	58	1.44	no	7.33
30	586			48 (2D6)	12	41	6.32		
31	<1	1.1	0.7	11 (2D6)	5	58	0.429	no	
32	<1		0.7	8 (2C9)	8	49	4.15		
33	<1			>50	8	43	>10		
34	<1	3		>50	5	38			
35	<1		1.2	>20	4	23	>3		
36	<1	0.1	6.5	>50	0	40	>2	no	
37	58	0.1	12	>50	9	23	>30	no	
38	<1		0.95	>50	3	6	>3	no	
39	<1				19	50			
40	<1	19	4	>50	14	36	4.1	yes	

[a]Lyophilized solubility assay. [b]Apical to basolateral CACO2 permeability, followed by measured efflux ratio. [c]Human plasma protein binding % free fraction. [d]CYP450 inhibition at isoforms 3A4, 2C9, and 2D6. Isoform with the highest percent inhibition listed. [e]Stability in human liver microsomes (mL/min/kg). [f]Stability in rat liver microsomes (mL/min/kg). [g]hERG channel binding. [h]GSH adduct formation flag. [i]Calculated pK_a, Moka Linux version 20090616 T.

solubility, this modification might also provide an opportunity to address the microsomal stability of the molecules compared to the dimethylpropylamine containing compounds. The dimethylpropylamine and other linear solubilizing pieces all tended to exhibit moderate to low microsomal stability, most likely due to *N*-demethylation at the terminal amine or *N*-dealkylation at the N1-position of the indazole. We hypothesized that an increase in the steric bulk around the N1 position might restrict the access of metabolizing enzymes to this site, and these new cycles would not have the *N*-demethylation problem. While we did see the desired improvements to microsomal stability, these changes tended to adversely affect human whole blood potency (Tables 4, 5).

The third approach to improve pharmacokinetic properties involved the reduction of the number of sp^2 centers (Table 4, compounds **39**−**40**). We, and others, have successfully used this strategy in the past to improve solubility of scaffolds.[6,18] Because the pyrrolopyrazine core acted as our kinase hinge binder, and the amide group was critical for potency, we felt our best option was to saturate one of the aromatic rings of the heterocyclic "selectivity" piece. We hoped that a partially saturated bicycle,

dx.doi.org/10.1021/jm301720p | J. Med. Chem. 2013, 56, 1677−1692

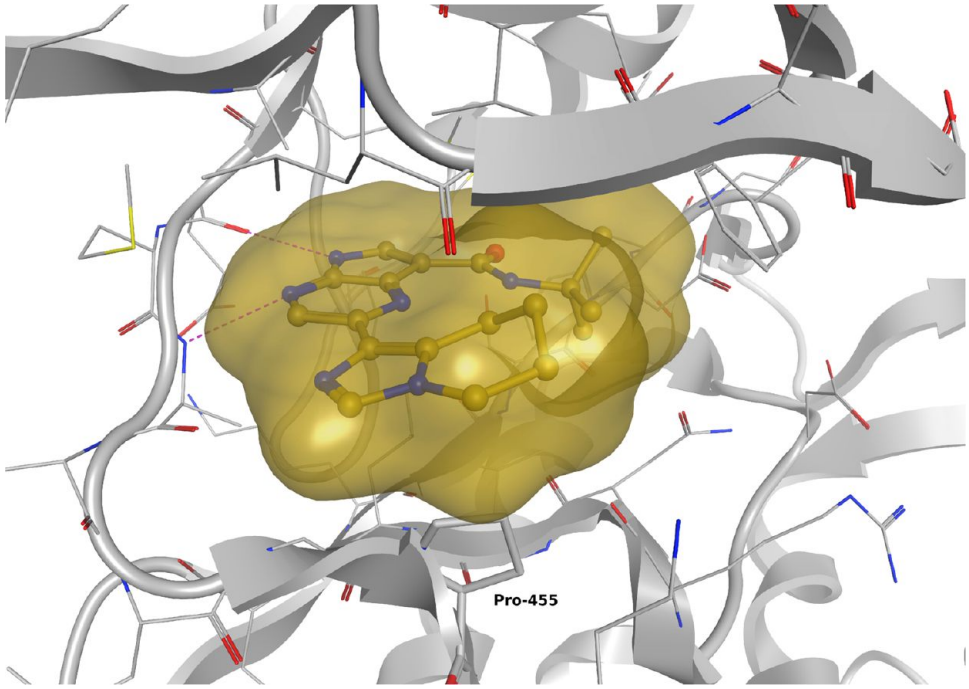

Figure 6. Crystal structure of compound **40** in complex with Syk (PDB accession number 4I0T, 1.7 Å resolution). Carbon atoms of the protein are colored in gray, and compound carbon atoms and molecular surface are colored in gold. Hydrogen bonds between protein (hinge atoms) and compound are highlighted in magenta.

Table 6. Inhibition of Syk Activity, Selectivity, B-Cell Potency, and Human Whole Blood Potency for Pyrrolopyrazines 41−43

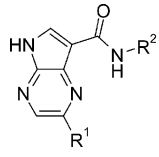

Compound	R^1	R^2	Syk IC_{50}[a] (nM)	Kinase Selectivity[b]	B cell IC_{50}[c] (μM)	HWB IC_{50}[d] (μM)
41	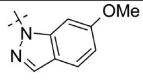	^{t}Bu	33	-	0.129	-
42	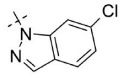		24	-	0.132	9.95
43	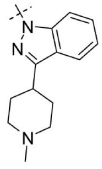		19	-	-	0.054

[a]See Experimental Section for details. [b]DiscoverX kinase screening dendrogram (number of kinases inhibited >90% at 10 μM). The KINOMEscan screening platform employs an active site-directed competition binding assay to quantitatively measure interactions between test compounds and multiple kinase assays. [c]Ramos B cell IC_{50}. [d]Human whole blood IC_{50}. [e]Calculated log *P*. [f]Tested at 1 μM concentration.

appropriately substituted, would continue to form favorable van der Waals interactions with Pro455. Unfortunately, none of these analogues showed improved solubility in our LYSA assay. Our prototype, pyrazole **39**, was highly permeable, and retained cell-based potency. Further improvements were realized when we switched from the pyrazole to the weakly basic imidazole (e.g., **40**). Despite the low solubility values in the LYSA assay, the pharmacokinetic properties were significantly enhanced, as is evident from the single dose PK data: **40** showed good oral bioavailability (Table 8). We also obtained a crystal structure which showed that the saturated ring of compound **40** was interacting favorably with the Pro455 (Figure 6). However, we

dx.doi.org/10.1021/jm301720p | *J. Med. Chem.* 2013, 56, 1677−1692

believe that these interactions are suboptimal because profiling determined that these compounds showed affinity for many other kinases. This, coupled with the discovery that several of these compounds were hERG inhibitors and showed GSH adduct formation, led us to halt further investigation.

A simultaneous effort involved the evaluation of regioisomeric scaffolds (Tables 6, 7; compounds **41**–**43**). Applying the same

Table 7. Solubility[a], Permeability[b], Human Plasma Protein Binding[c], CYP450 Inhibition[d], and Liver Microsomal Stability[e,f], hERG Channel Inhibition[g], and GSH-Adduct Formation[h]

compd	LYSA[a] (μg/mL)	CACO2 AB (ER)[b]	CYP450 IC_{50} (μM)[d]	HLM[e]	RLM[f]	hERG IC_{50}[g] (μM)	GSH[h]
41	<1		>8 (2C9)	11	37		
42	<1		>19	14	35		no
43	19	0.3	12 (2D6)	7	42	>10	no

[a]Lyophilized solubility assay. [b]Apical to basolateral CACO2 permeability, followed by measured efflux ratio. [c]Human plasma protein binding % free fraction. [d]CYP450 inhibition at isoforms 3A4, 2C9 and 2D6. Lowest inhibition value indicated. [e]Stability in human liver microsomes (mL/min/kg). [f]Stability in rat liver microsomes (mL/min/kg). [g]hERG channel binding. [h]GSH adduct formation flag.

SAR learnings from the main series, we were able to generate compounds with exceptionally good potency. The discovery that these N-linked indazoles could also offer highly potent Syk inhibitors did represent an important finding that led to the identification of a new subseries. The details of these ongoing efforts to identify safe, selective Syk inhibitors will be the subject of future communications.

In evaluating all the compounds made in this series with respect to overall best profiles, we selected compound **24** for IP dosing in rodents in order to reach a decision as to whether to continue to pursue this scaffold. We envisioned that if we could show efficacy with this compound, the basic amine would permit us to use a pro-drug strategy to improve oral PK behavior. Compound **24** did show good IP single dose PK (5 mg/kg), and we evaluated this compound further in our in vivo efficacy model. Unfortunately, very soon after repeat dosing at 100, 30, and 10 mg/kg in our mouse model (collagen induced arthritis), the compound showed toxicity that precluded us from continuing the study. The etiology of this toxicity was not determined but was of sufficient concern to us that we decided that this scaffold should be deprioritized.

CONCLUSIONS

We demonstrated that seeking to optimize the interaction between ATP-competitive Syk inhibitors and a specific Pro455 residues constitutes a reliable approach toward the discovery of drug candidates with high levels of Syk specificity and potency. Molecular modeling was used to explore ways to achieve the requisite interactions with Pro455, and ultimately we found that incorporation of an indazole moiety provided excellent selectivity over the kinome. Furthermore, an increase in the steric bulk at the amide portion produced favorable increases in potency and selectivity, particularly over the JAK family of kinases. We demonstrated that a reduction of lipophilicity improved HWB potency, a predictor for efficacy in the clinic. We also successfully improved solubility, but despite this we were unable to improve oral bioavailability. Intraperitoneal dosing to assess the viability of the scaffold led to the discovery of unexpected toxicity, which ultimately led to the deprioritization of this series in favor of more soluble starting points with improved PK properties.

EXPERIMENTAL SECTION

Chemistry. Compounds **6**–**43** were prepad following one of the general synthetic schemes (Schemes 1, 2, 3, 4, and 5) below:

Scheme 1. General Synthetic Scheme 1

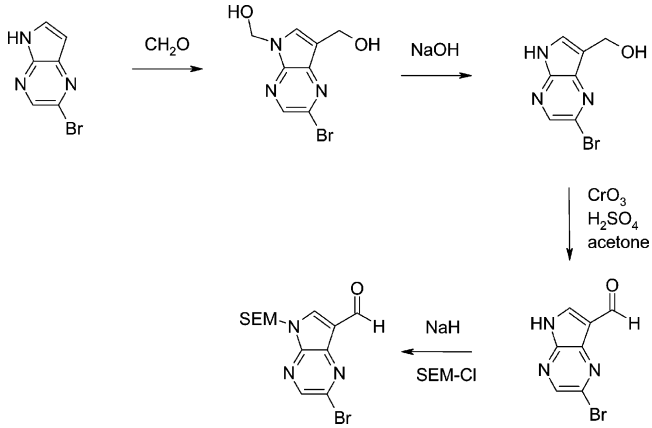

General Methods. All reagents and solvents were purchased from commercial sources and used without further purification. ^{1}H NMR spectra were measured using a Bruker NMR Avance 400 MHz or Bruker NMR Avance 300 MHz spectrometer, and chemical shifts were expressed in δ (ppm) units using tetramethylsilane as an internal standard (in ^{1}H NMR description: s = singlet, d = doublet, t = triplet, q = quartet, m = multiplet, and br = broad peak). Mass spectra were recorded on and Agilent AG1 Single Quad G6140A spectrometer.

Purity values for all tested compounds were found to be above 95% from the high-performance liquid chromatography (HPLC) analyses. In general, the nomenclature used in this section is based on AUTONOMTM v.4.0, as noted above, or, alternatively, based on ChemDraw. Protein crystal structures were determined as described previously.[19] Commonly used abbreviations: acetyl (Ac), atmospheres (Atm), *tert*-butoxycarbonyl (Boc), benzyl (Bn), butyl (Bu), benzyloxycarbonyl (CBZ or Z), dibenzylideneacetone (dba), dichloromethane (DCM), di-*iso*-butylaluminumhydride (DIBAL or DIBAL-H), di-*iso*-propylethylamine (DIPEA), 4-*N*,*N*-dimethylaminopyridine (DMAP),

Table 8. Single-Dose Pharmacokinetic Parameters in Mouse of Selected Compounds[a]

compd	species	CLiv (mL/min/kg)	$T_{1/2\ h}$	Vd_{ss} (L/kg)	AUC/dose (ng/mL·h/(mg/kg))	*F* (%)
15	rat	25.8	0.71	3.7	3.07	0.5
18	rat	44.2	4.93	8.4	5.69	2.2
24	rat (po)	55.6	5.33	24.4	0	0
24	mouse (ip)	NA	NA	NA	286	NA
40	rat	48.8	0.52	1.73	3.76	100

[a]*n* = 2–3 per time point. IV dose = 0.5 or 1 mg/kg. PO dose = 10 or 20 mg/kg. IP dose = 5 mg/kg.

dx.doi.org/10.1021/jm301720p | J. Med. Chem. 2013, 56, 1677–1692

Scheme 2. General Synthetic Scheme 2

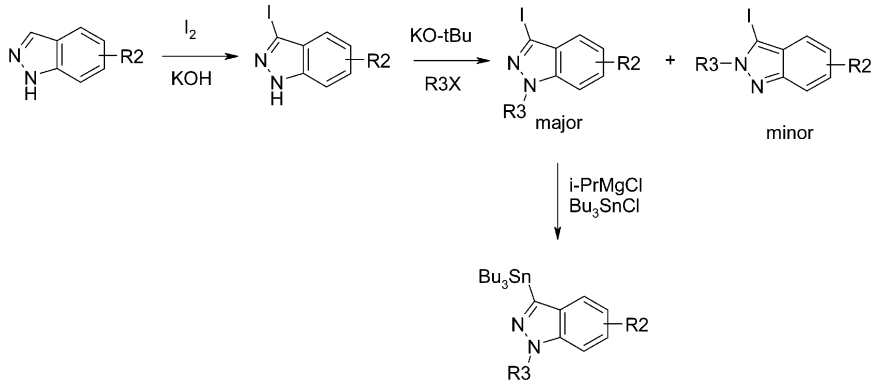

Scheme 3. General Synthetic Scheme 3

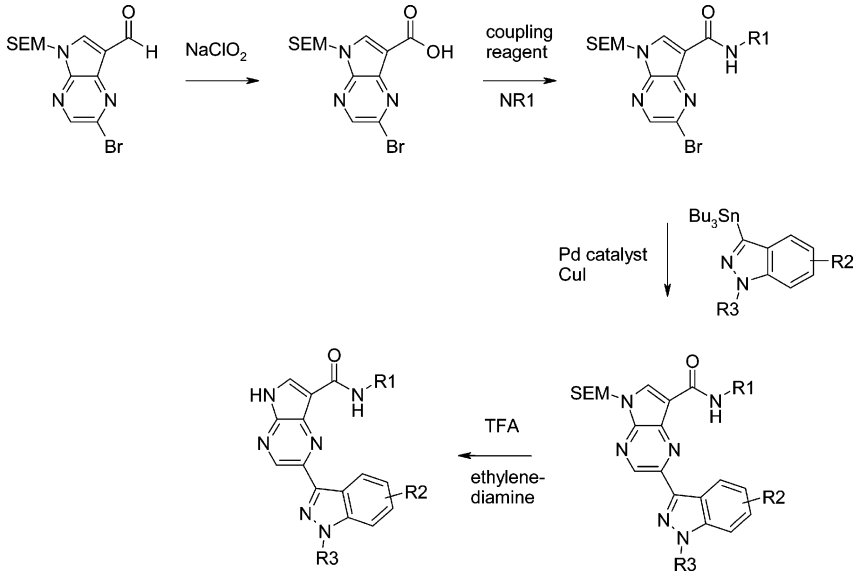

N,*N*-dimethylformamide (DMF), dimethyl sulfoxide (DMSO), 1,1′-bis-(diphenylphosphino)ferrocene (dppf), 1-(3-dimethylaminopropyl)-3-ethylcarbodiimide hydrochloride (EDCI), ethylenediaminetetraacetic acid (EDTA), ethyl (Et), ethyl acetate (EtOAc), ethanol (EtOH), diethyl ether (Et_2O), *O*-(7-azabenzotriazole-1-yl)-*N*,*N*,*N*′*N*′-tetramethyluronium hexafluorophosphate acetic acid (HATU), 1-*N*-hydroxybenzotriazole (HOBt), high pressure liquid chromatography (HPLC), liquid chromatography−mass spectrometry (LCMS), methanol (MeOH), melting point (mp or MP), methyl (Me), mass spectrum (ms or MS), *N*-methylmorpholine (NMM), *N*-methylpyrrolidone (NMP), phenyl (Ph), propyl (Pr), *iso*-propyl (*i*-Pr), pyridine (pyr), room temperature (rt or RT), triethylamine (TEA or Et_3N), trifluoroacetic acid (TFA), thin layer chromatography (TLC), and tetrahydrofuran (THF). Conventional nomenclature including the prefixes *normal* (*n*), *iso* (*i*-), *secondary* (*sec*-), *tertiary* (*tert*-), and *neo*- have their customary meaning when used with an alkyl moiety.[20]

The preparation of **9** represents a typical procedure used for the synthesis of the pyrrolopyrazines.

*N-tert-Butyl-2-(6-chloro-1-methyl-1H-indazol-3-yl)-5H-pyrrolo-[2,3-b]pyrazine-7-carboxamide **9**.*

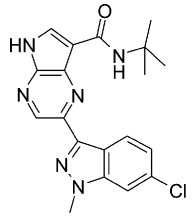

Step 1. *(2-Bromo-7-hydroxymethyl-pyrrolo[2,3-b]pyrazin-5-yl)-methanol **50**.*

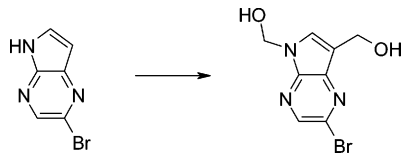

To a suspension of 2-bromo-5*H*-pyrrolo[2,3-*b*]pyrazine (5.0 g, 25.2 mmol) in 1,4-dioxane (100 mL) was added 2.0 M aqueous NaOH (25 mL, 50.0 mmol) and 37% aqueous formaldehyde (19 mL, 252 mmol). The dark homogeneous reaction mixture was stirred at room temperature overnight. The organics were evaporated under reduced pressure. The aqueous layer was neutralized with 1.0 M HCl and extracted with EtOAc (2×). The combined organics were concentrated to afford 2.6 g of an orange solid. Upon standing, a thick brown precipitate formed in the aqueous layer. The precipitate was collected by filtration and dried. The brown solid was extracted with hot 10% MeOH/EtOAc (3 × 200 mL). The extracts were combined and evaporated to provide an additional 3.05 g of orange solid to yield **50** (5.65 g, 87%). LCMS $(M + H)^+ = 258, 260$. ^1H NMR (DMSO-d_6, 400 MHz) δ: 8.43 (s, 1H), 7.96 (s, 1H), 6.71 (t, $J = 7.3$ Hz, 1H), 5.59 (d, $J = 7.6$ Hz, 2H), 5.10 (t, $J = 5.3$ Hz, 1H), 4.66 (d, $J = 5.6$ Hz, 2H).

dx.doi.org/10.1021/jm301720p | J. Med. Chem. 2013, 56, 1677−1692

Scheme 4. General Synthetic Scheme 4

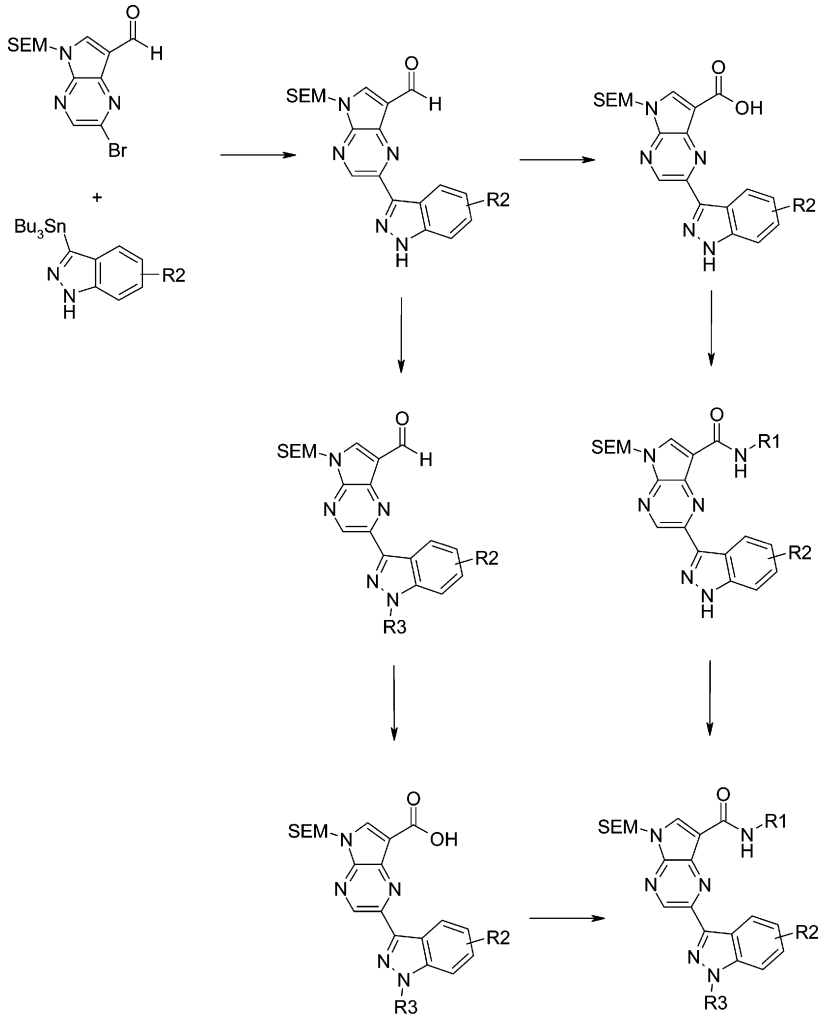

Scheme 5. General Synthetic Scheme 5

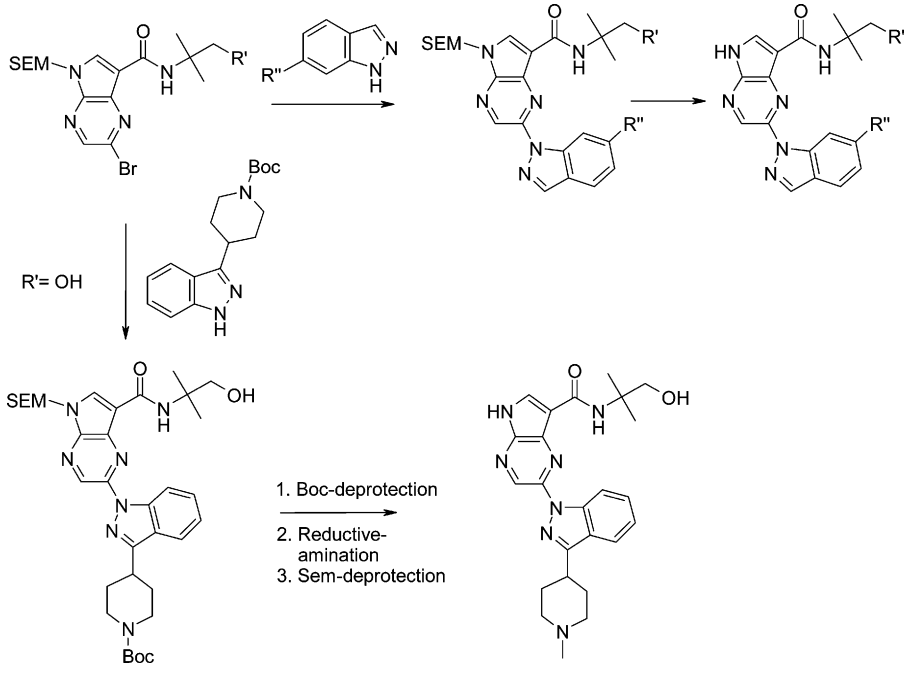

dx.doi.org/10.1021/jm301720p | J. Med. Chem. 2013, 56, 1677−1692

Step 2. *(2-Bromo-5H-pyrrolo[2,3-b]pyrazin-7-yl)-methanol* ***51***.

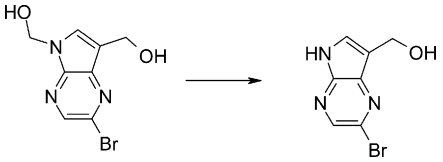

To a suspension of **50** (5.65 g, 21.9 mmol) in THF (150 mL) was added a solution of 2.0 M aqueous NaOH (33 mL, 66 mmol). The homogeneous reaction mixture was stirred overnight, and then the organics were removed under reduced pressure. The aqueous residue was brought to pH 4 with 1.0 M aqueous HCl. The resulting precipitate was collected by filtration and rinsed with H_2O to afford 3.68 g of a yellow solid. The filtrate was extracted with EtOAc (2×), and the organics were concentrated under reduced pressure to provide an additional 0.92 g of yellow solid to yield **51** (4.60 g, 92%). ^{1}H NMR (DMSO-d_6, 300 MHz) δ: 12.19 (br s, 1H), 8.33 (s, 1H), 7.85 (s, 1H), 4.96 (t, J = 5.3 Hz, 1H), 4.62 (d, J = 4.9 Hz, 2H).

Step 3. *2-Bromo-5-(2-trimethylsilanyl-ethoxymethyl)-5H-pyrrolo-[2,3-b]pyrazine-7-carbaldehyde* ***52***.

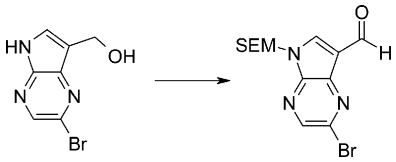

A stock solution of Jones reagent (2.67 M) was prepared by carefully adding concentrated H_2SO_4 (2.3 mL) to CrO_3 (2.67 g) amd then diluting to 10 mL with H_2O. To a suspension of **51** (4.6 g, 20.1 mmol) in acetone (300 mL) was slowly added Jones reagent (9 mL, 24.0 mmol). During the addition, the starting material gradually dissolved and a thick green solid was formed. The reaction mixture was stirred for 15 min and then quenched with *i*-PrOH (2 mL) and filtered over Celite, rinsing with acetone. The filtrate was concentrated to provide 4.76 g of 2-bromo-5*H*-pyrrolo[2,3-*b*]pyrazine-7-carbaldehyde as a yellow−orange solid that was used without further purification. To a solution of this solid in DMF (50 mL) at 0 °C was added NaH (60% in mineral oil, 1.2 g, 30.1 mmol). The reaction mixture was stirred at room temperature for 30 min and then cooled back to 0 °C, and 2-(trimethylsilyl)ethoxymethyl chloride (4.3 mL, 24.1 mmol) was slowly added. The reaction mixture was warmed to room temperature and stirred for 1 h and then quenched with H_2O and extracted with EtOAc (3×). The combined organics were washed with H_2O (3×) and brine and then dried over $MgSO_4$ and concentrated. The residue was purified by flash chromatography eluting with 20−30% EtOAc/hexanes to give **52** (3.82 g, 53%) as a yellow solid. ^{1}H NMR ($CDCl_3$, 300 MHz) δ: 10.37 (s, 1H), 8.50 (s, 1H), 8.33 (s, 1H), 5.73 (s, 2H), 3.53−3.70 (m, 2H), 0.90−1.05 (m, 2H), 0.00 (s, 9H).

Step 4. *6-Chloro-3-iodo-1H-indazole* ***53***.

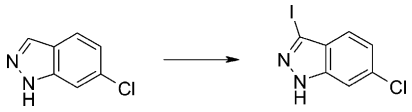

In a round-bottomed flask, 6-chloro-1*H*-indazole (90 mg, 0.59 mmol, available commercially from Ark Pharm, Inc.) was dissolved in DMF (1.4 mL). Iodine (300 mg, 1.18 mmol) was added, followed by potassium hydroxide (128 mg, 2.28 mmol). The dark reaction mixture was stirred at room temperature for 3 h and then was quenched with 10% aqueous $NaHSO_3$ and extracted with diethyl ether (2×). The combined organic layers were washed with water and brine and then dried over sodium sulfate, filtered, and concentrated to give **53** (169 mg, 98%) as an orange solid. ^{1}H NMR (chloroform-*d*) δ: 7.52 (d, J = 1.5 Hz, 1H), 7.46 (s, 1H), 7.44 (s, 1H), 7.23 (d, J = 1.5 Hz, 1H), 7.20 (d, J = 1.5 Hz, 1H)

Step 5. *6-Chloro-3-iodo-1-methyl-1H-indazole* ***54***.

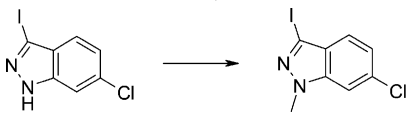

In a round-bottomed flask, **53** (167 mg, 0.57 mmol) was dissolved in THF (2 mL) and the solution was cooled to 0 °C. Potassium *tert*-butoxide (90 mg, 0.80 mmol) was added, and the reaction mixture was stirred at 0 °C for 1.25 h. Methyl iodide (0.045 mL, 0.72 mmol) was added dropwise and then the ice bath was removed and the reaction mixture was stirred at room temperature for 2 h. The reaction mixture was quenched with water and extracted with EtOAc (2×). The combined organic layers were washed with water and brine and then dried over sodium sulfate, filtered, and concentrated. The residue was purified by flash chromatography eluting with 0−5% EtOAc/hexanes to afford **54** (110 mg, 63%) as a yellow solid. ^{1}H NMR (DMSO-d_6) δ: 7.91 (dd, J = 1.8, 0.5 Hz, 1H), 7.44 (dd, J = 8.7, 0.6 Hz, 1H), 7.22 (dd, J = 8.5, 1.8 Hz, 1H), 4.05 (s, 3H).

Step 6. *6-Chloro-1-methyl-3-tributylstannanyl-1H-indazole* ***55***.

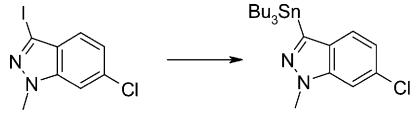

Compound **54** (108 mg, 0.35 mmol) was dissolved in THF (2 mL), and the solution was cooled to −16 °C using a NaCl/ice bath. Isopropylmagnesium chloride (2.0 M in THF, 0.20 mL, 0.40 mmol) was added dropwise, and the reaction mixture was stirred at −16 °C for 15 min. Tributylchlorostannane (0.11 mL, 0.40 mmol) was slowly added, and the reaction mixture was allowed to warm to room temperature over 1.5 h. The reaction mixture was quenched with saturated NH_4Cl solution and extracted with EtOAc (2×). The combined organic layers were washed with water and brine and then dried over sodium sulfate, filtered, and concentrated to afford **55** as a brown oil, which was used immediately into the next step without further purification.

Step 7. *2-(6-Chloro-1-methyl-1H-indazol-3-yl)-5-(2-trimethylsilanyl-ethoxymethyl)-5H-pyrrolo[2,3-b]pyrazine-7-carbaldehyde* ***56***.

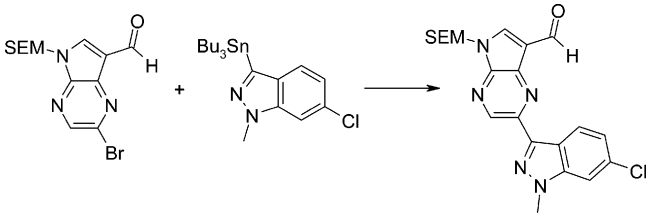

In a round-bottomed flask, **52** (400 mg, 1.12 mmol) and **55** (1.11 g, 1.7 mmol) were dissolved in DMF (10 mL). The flask was evacuated and backfilled with argon, and then tetrakis(triphenylphosphine)palladium (0) (65 mg, 0.056 mmol) and copper(I) iodide (43 mg, 0.23 mmol) were added. The reaction mixture was stirred at 80 °C in an oil bath overnight and then cooled to room temperature, quenched with water, and extracted with diethyl ether (2×). The combined organic layers were washed twice with water and once with brine and then dried over sodium sulfate, filtered, and concentrated. The residue was adsorbed on silica gel and purified by flash chromatography eluting with 0−30% EtOAc/hexanes to give **56** (416 mg, 84%) as a yellow solid. ^{1}H NMR (chloroform-*d*) δ: 10.52 (s, 1H), 9.33 (s, 1H), 8.78 (d, J = 8.7 Hz, 1H), 8.33 (s, 1H), 7.49 (s, 1H), 7.34 (dd, J = 8.7, 1.5 Hz, 1H), 5.80 (s, 2H), 4.19 (s, 3H), 3.58−3.77 (m, 2H), 0.91−1.05 (m, 2H), 0.00 (s, 9H).

Step 8. *2-(6-Chloro-1-methyl-1H-indazol-3-yl)-5-(2-trimethylsilanyl-ethoxymethyl)-5H-pyrrolo[2,3-b]pyrazine-7-carboxylic Acid* ***57***.

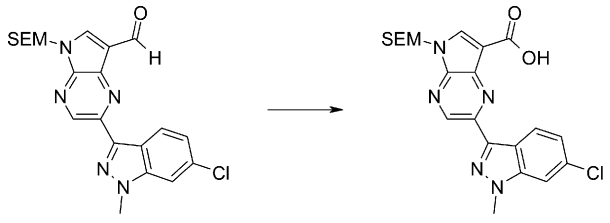

In a round-bottomed flask, **56** (412 mg, 0.93 mmol) was suspended in 1,4-dioxane (15 mL) and water (3 mL). The suspension was cooled to 0 °C, and sulfamic acid (543 mg, 5.59 mmol) was added. Then, a solution of sodium chlorite (80%, 137 mg, 1.21 mmol) and potassium dihydrogen phosphate (1.52 g, 11.2 mmol) in water (9 mL) was added

dx.doi.org/10.1021/jm301720p | J. Med. Chem. 2013, 56, 1677−1692

via dropping funnel over 20 min. After the addition was complete, the ice bath was removed and the reaction mixture was stirred at room temperature for 3 h. THF (15 mL) was added, and the reaction mixture was stirred at room temperature for an additional 3 h. The reaction mixture was diluted with water and extracted with EtOAc (2×). The combined organic layers were washed with water and brine and then dried over sodium sulfate, filtered, and concentrated. The residue was triturated with ethyl acetate/hexanes to afford **57** (358 mg, 84%) as a light-yellow powder. ^{1}H NMR (chloroform-*d*) δ: 9.37 (s, 1H), 8.42 (t, J = 4.3 Hz, 2H), 7.52 (d, J = 1.5 Hz, 1H), 7.34 (dd, J = 8.5, 1.7 Hz, 1H), 5.79 (s, 2H), 4.20 (s, 3H), 3.52−3.75 (m, 2H), 0.93−1.06 (m, 2H), 0.00 (s, 9H).

Step 9. *N-tert-Butyl-2-(6-chloro-1-methyl-1H-indazol-3-yl)-5H-pyrrolo[2,3-b]pyrazine-7-carboxamide* ***9***. To a stirred suspension of

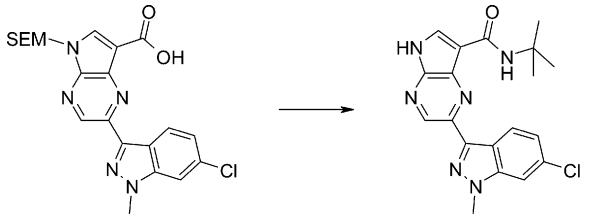

57 (111 mg, 242 μmol) in DMF (4 mL) was added EDC (107 mg, 557 μmol), HOBT (107 mg, 557 μmol), and 2-methylpropan-2-amine (78.6 mg, 0.113 mL, 1.08 mmol) at 20 °C. After 3 h, the reaction mixture was diluted with ethyl acetate, washed with 10% citric acid solution, saturated sodium bicarbonate, and brine and then dried (sodium sulfate), filtered, and concentrated in vacuo. Crude *N-tert*-butyl-2-(6-chloro-1-methyl-1*H*-indazol-3-yl)-5-((2-(trimethylsilyl)ethoxy)-methyl)-5*H*-pyrrolo[2,3-*b*]pyrazine-7-carboxamide (140 mg, 273 μmol) was dissolved in dichloromethane (5 mL), and to this solution was added trifluoroacetic acid (3.11 g, 2.1 mL, 27.3 mmol) at 20 °C. After 6 h, the mixture was concentrated in vacuo. The residue was suspended in dichloromethane (5 mL) and ethylenediamine (1.23 g, 1.38 mL, 20.5 mmol) added and the mixture stirred at room temperature for 15 h and then concentrated in vacuo. The solid residue was triturated with water, separated by filtration, dried, and then purified by flash chromatography eluting with 0−5% methanol in dichloromethane to give **9** (63 mg, 60%) as a pale-yellow powder. LCMS $(M + Na)^+$ = 405. ^{1}H NMR ($CDCl_3$) δ: 11.84 (br s, 1H), 9.05 (s, 1H), 8.38 (d, J = 8.7 Hz, 1H), 8.14 (d, J = 3.4 Hz, 1H), 7.96 (s, 1H), 7.39 (d, J = 1.5 Hz, 1H), 7.08 (dd, J = 8.5, 1.7 Hz, 1H), 4.04 (s, 3H), 1.48 (s, 9H).

■ ASSOCIATED CONTENT

Ⓢ Supporting Information

Full experimental detail and characterization of all new synthetic intermediates and final products along with experimental procedures for the Syk biochemical and cell-based assays. This material is available free of charge via the Internet at http://pubs.acs.org.

■ AUTHOR INFORMATION

Corresponding Author

*For F.P.: phone, (973) 235-7319; E-mail, fernando.padilla@roche.com. For M.C.L.: phone, (408) 585-8051; E-mail, mattlucas70@hotmail.com.

Present Addresses

[§]Cubist Pharmaceuticals, 65 Hayden Avenue, Lexington, Massachusetts 02421, United States.

[∥]Principia BioPharma, Inc., 400 E. Jamie Court #302, South San Francisco, California 94080, United States.

[⊥]School of Pharmaceutical Sciences, Soochow University, 199 Ren Ai Rd. Suzhou, Jiangsu, P.R.China.

Notes

The authors declare no competing financial interest.

■ ACKNOWLEDGMENTS

We thank Karen Lackey, Satwant Narula and Julie DeMartino for their guidance and strategic discussions.

■ ABBREVIATIONS USED

ATP, adenosine triphosphate; Btk, Bruton's tyrosine kinase; CD69, cluster of differentiation 69; GSH, glutathione; hERG, human ether-a-go-go-related gene; HLM, human liver microsomes; HWB, human whole blood; IP, intraperitoneally; ITP, idiopathic thrombocytopenic purpura; Jak, Janus kinase; LYSA, lyophilized solubility assay; PK, pharmacokinetics; PPB, plasma protein binding; RA, rheumatoid arthritis; RLM, rat liver microsomes; SDPK, single dose pharmacokinetics; SLE, systemic lupus erythematous; Syk, spleen tyrosine kinase

■ REFERENCES

(1) Lawrence, D. S.; Niu, J. Protein Kinase Inhibitors: The Tyrosine-Specific Protein Kinases. *Pharmacol. Ther.* **1998**, *77*, 81−114.

(2) Mócsai, A.; Ruland, J.; Tybulewicz, V. L. J. The SYK tyrosine kinase: a crucial player in diverse biological functions. *Nature Rev. Immunol.* **2010**, *10*, 387−402.

(3) Pamuk, O. N.; Tsokos, G. Spleen tyrosine kinase inhibition in the treatment of autoimmune, allergic and autoinflammatory diseases. *Arthritis Res. Ther.* **2010**, *12*, 222.

(4) Taniguchi, T.; Kobayashi, T.; Kondo, J.; Takahashi, K.; Nakamura, H.; Suzuki, J.; Nagai, K.; Yamada, T.; Nakamura, S.; Yamamura, H. Molecular cloning of a porcine gene Syk that encodes a 72-kDa protein−tyrosine kinase showing high susceptibility to proteolysis. *J. Biol. Chem.* **1991**, *266*, 15790−15796.

(5) Riccaboni, M.; Bianchi, I.; Petrillo, P. Spleen tyrosine kinases: biology, therapeutic targets and drugs. *Drug Discovery Today* **2010**, *15*, 517−530.

(6) Kyttaris, V. C.; Tsokos, G. C. Syk kinase as a treatment target for therapy in autoimmune diseases. *Clin. Immunol.* **2007**, *124*, 235−237.

(7) Wong, B. R.; Grossbard, E. B.; Payan, D. G.; Masuda, E. S. Targeting Syk as a treatment for allergic and autoimmune disorders. *Expert Opin. Invest. Drugs* **2004**, *13*, 743−762.

(8) (a) Tam, F. W. K.; McAdoo, S. P. Fostamatinib disodium. *Drugs Future* **2011**, *36*, 273−280. (b) Weinblatt, M. E.; Kavanaugh, A.; Genovese, M. C.; Musser, T. K.; Grossbard, E. B.; Magilavy, D. B. An oral spleen tyrosine kinase (Syk) inhibitor for rheumatoid arthritis. *N. Engl. J. Med.* **2010**, *363*, 1303−1312.

(9) Lucas, M.; Goldstein, D.; Hermann, J.; Kuglstatter, A.; Liao, C.; Liu, W.; Padilla, F.; Slade, M.; Wanner, J.; Xie, W.; Zhang, X.; Luk, K. C. Rational design of highly selective spleen tyrosine kinase inhibitors. *J. Med. Chem.* **2012**, *55*, 10414−10423.

(10) Coffey, G.; DeGuzman, F.; Inagaki, M.; Pak, Y.; Delaney, S. M.; Ives, D.; Betz, A.; Jia, Z. J.; Pandey, A.; Baker, D.; Hollenbach, S. J.; Phillips, D. R.; Sinha, U. Specific Inhibition of Spleen Tyrosine Kinase Suppresses Leukocyte Immune Function and Inflammation in Animal Models of Rheumatoid Arthritis. *J. Pharmacol. Exp. Ther.* **2012**, *34*, 350−359.

(11) (a) Hendricks, R. T.; Hermann, J. C.; Jaime-Figueroa, S.; Kondru, R. K.; Lou, Y.; Lynch, S. M.; Owens, T. D.; Soth, M.; Yee, C. W. Pyrrolo[2,3-*b*]pyrazine-7-carboxamide derivatives as JAK and SYK inhibitors and their preparation and use for the treatment of autoimmune and inflammatory diseases. Patent WO 2011144585, 2011; (b) Hendricks, R. T.; Hermann, J.; Kondru, R.; Lou, Y.; Lynch, S. M.; Owens, T. D.; Soth, M. Preparation of pyrrolopyrazine as kinase inhibitors useful for the treatment of autoimmune and inflammatory diseases. U.S. Patent US 20110230462, 2011; (c) Bamberg, J. T.; Bartlett, M.; Dubois, D. J.; Elworthy, T. R.; Hendricks, R. T.; Hermann, J. C.; Kondru, R. K.; Lemoine, R.; Lou, Y.; Owens, T. D.; Park, J.; Smith, D. B.; Soth, M.; Yang, H.; and Yee, C. W. Preparation of pyrrolopyrazines as JAK and SYK inhibitors. U.S. Patent US 20090215750, 2009; (d) Dubois, D. J.; Hendricks, R. T.; Hermann, J. C.; Kondru, R. K.; Lou, Y.; Owens, T. D.; Yee, C. W. Preparation of

pyrrolopyrazines as JAK and SYK inhibitors. U.S. Patent US 20090215724, 2009.
(12) Lynch, S. M.; DeVicente, J.; Hermann, J. C.; Jaime-Figueroa, S.; Jin, S.; Kuglstatter, A.; Li, H.; Lovey, A.; Menke, J.; Niu, L.; Patel, V.; Roy, D.; Soth, M.; Steiner, S.; Tivitmahaisoon, P.; Vu, M. D. and Yee, C. Identification of Potent, Selective JAK3 Inhibitors through Structure Based Design and Strategic use of Conformational Bias. *Bioorg. Med. Chem. Lett.* submitted for publication.
(13) *Molecular Operating Environment (MOE), 2011.10*; Chemical Computing Group Inc.: 1010 Sherbooke St. West, Suite #910, Montreal, QC H3A 2R7, Canada, 2011.
(14) Garber, K. Pfizer's JAK inhibitor sails through phase 3 in rheumatoid arthritis. *Nature Biotechnol.* **2011**, *29*, 467.
(15) Cubeddu, L. X. Iatrogenic QT Abnormalities and Fatal Arrhythmias: Mechanisms and Clinical Significance. *Curr. Cardiol. Rev.* **2009**, *5*, 166−176.
(16) (a) Cumming, J. G.; Tucker, H.; Oldfield, J.; Fielding, C.; Highton, A.; Faull, A.; Wild, M.; Brown, D.; Wells, S.; Shaw, J. Balancing hERG affinity and absorption in the discovery of AZD5672, an orally active CCR5 antagonist for the treatment of rheumatoid arthritis. *Bioorg. Med. Chem. Lett.* **2012**, *22*, 1655−1659. (b) Shultz, M. D.; Cao, X.; Chen, C. H.; Cho, Y. S.; Davis, N. R.; Eckman, J.; Fan, J.; Fekete, A.; Firestone, B.; Flynn, J.; Green, J.; Growney, J. D.; Holmqvist, M.; Hsu, M.; Jansson, D.; Jiang, L.; Kwon, P.; Liu, G.; Lombardo, F.; Lu, Q.; Majumdar, D.; Meta, C.; Perez, L.; Pu, M.; Ramsey, T.; Remiszewski, S.; Skolnik, S.; Traebert, M.; Urban, L.; Uttamsingh, V.; Wang, P.; Whitebread, S.; Whitehead, L.; Yan-Neale, Y.; Yao, Y.-M.; Zhou, L.; Atadja, P. Optimization of the in vitro cardiac safety of hydroxamate-based histone deacetylase inhibitors. *J. Med. Chem.* **2011**, *54*, 4752−4772. (c) Mendez-Andino, J. L.; Wos, J. A. MCH-R1 antagonists: what is keeping most research programs away from the clinic? *Drug Discovery Today* **2007**, *12*, 972. (d) Rokosz, L. L.; Hobbs, D. W. Biological Examination of Melanin Concentrating Hormone Receptor 1: Multi-tasking from the Hypothalamus. *Drug News Perspect.* **2006**, *19*, 273.
(17) Perry, M.; Stansfeld, P. J.; Leaney, J.; Wood, C.; de Groot, M. J.; Leishman, D.; Sutcliffe, M. J.; Mitcheson, J. S. Drug binding interactions in the inner cavity of HERG channels: molecular insights from structure−activity relationships of clofilium and ibutilide analogs. *Mol. Pharmacol.* **2006**, *69*, 509−519.
(18) Ritchie, T. J.; Macdonald, S. J. F.; Young, R. J.; Pickett, S. D. The impact of aromatic ring count on compound developability: further insights by examining carbo- and hetero-aromatic and aliphatic ring types. *Drug Discovery Today* **2011**, *16*, 164−171.
(19) Villaseñor, A. G.; Kondru, R.; Ho, H.; Wang, S.; Papp, E.; Shaw, D.; Barnett, J. W.; Browner, M. F.; Kuglstatter, A. Structural Insights for Design of Potent Spleen Tyrosine Kinase Inhibitors from Crystallographic Analysis of Three Inhibitor Complexes. *Chem. Biol. Drug Des.* **2009**, *73*, 466−470.
(20) Rigaudy, J.; Klesney, D. P. *Nomenclature in Organic Chemistry: IUPAC*; Pergamon Press: Oxford, 1979.